applied optics

Photonic approach for simultaneous measurement of microwave DFS and AOA

JIANING ZHAO, ZHENZHOU TANG,* AND SHILONG PAN

Key Laboratory of Radar Imaging and Microwave Photonics, Ministry of Education, Nanjing University of Aeronautics and Astronautics, Nanjing 210016, China
*Corresponding author: tangzhzh@nuaa.edu.cn

Received 17 February 2021; revised 28 April 2021; accepted 28 April 2021; posted 30 April 2021 (Doc. ID 422946); published 24 May 2021

A photonic scheme that can simultaneously estimate the microwave Doppler-frequency shift (DFS) and angle-of-arrive (AOA) is demonstrated. In the proposed system, the transmitted signal is independently mixed with two echo signals by a dual-channel microwave photonic mixer. By measuring the frequency of the intermediate frequency (IF) signal output from the two channels and the phase difference between them, the DFS (with direction identification) and AOA parameters can be obtained. In a proof-of-concept experiment, the errors are less than ± 0.08 Hz for the DFS measurement within a range of ±100 kHz and less than ±1.3 deg for the AOA measurement ranging from 0° to 90°, respectively.

https://doi.org/10.1364/AO.422946

1. INTRODUCTION

Obtaining the distance, speed, and angle of moving objects is essential in the fields of intelligent driving [1], wireless communication [2,3], radar ranging [4–7], and medical imaging [8]. Generally, the determination of these parameters can be translated to the measurement of the Doppler frequency shift (DFS) and the angle of arrival (AOA). Due to the electronic bottlenecks, however, the conventional electronic measurement technologies are difficult to implement when the signal-under-test ranges from several MHz to even subterahertz. Recently, owing to the inherent advantages of large instantaneous bandwidth, low transmission loss, and immunity to electromagnetic interference, lots of photonics-based methods are reported to realize the measurements of microwave DFS and AOA [9–13]. For example, the microwave DFS can be simply measured by a microwave photonic mixer [14,15]. To distinguish the direction of the DFS, a reference RF signal (introduced by an acousto-optic modulator) [16] or an additional microwave source [17,18] or an auxiliary phase difference (realized by a photonic I/Q mixer [19]) is usually employed. On the other hand, different methods are applied to measure the AOA [20–25]. For instance, in [20], AOA is transferred to the coherent time delay, which can be acquired through measuring the notch frequency of the transmission response. Besides, AOA can also be obtained by measuring the optical power [21], the output DC voltage of a single-polarization system [22], or the DC voltage ratio of a dual-polarization system [23].

Most of the previously reported schemes can measure either DFS or AOA, not both. To simultaneously obtain the DFS and AOA, Li *et al*. proposed an approach based on a parallel microwave phonic mixer [24], which obtains the DFS from the frequency of the intermediate frequency (IF) signals after down-conversion as well as the AOA from the phase difference between them. However, data from the perpendicular bisector of the two receiving antennas cannot be obtained. To solve this problem, a polarization-division-multiplexed microwave photonic I/Q mixing system is employed [25]; however, the system structure is complicated. More recently, a simple photonics-based DFS and AOA estimation system is realized by a single fiber link [26], in which the DFS is obtained by adding a reference signal [18], and the AOA is calculated by measuring the power of the IF signal. However, this scheme needs an additional microwave source and has strict requirements on the carrier–suppression ratio, phase imbalance of the optical coupler, and precise bias of the modulator.

In this paper, a dual-channel microwave photonic mixer is employed to simultaneously measure the microwave DFS and AOA. In the proposed system, an optical carrier is sent to the polarization-division-multiplexed dual-drive Mach–Zehnder modulator (PDM-DMZM). A pair of transmitted signals are, respectively, fed into the RF ports of the two sub-DMZMs, and a pair of echo signals from different directions are separately sent to the other RF ports of the sub-DMZMs. The +1st-order sidebands are then selected using an optical bandpass filter (OBPF) and re-divided into two orthogonally polarized branches. After photodetection, a pair of IF signals with a specific phase relationship is obtained. By measuring the frequency and the phase relationship, the DFS (with direction) and AOA can be obtained. An experiment is carried out. The DFS with an error of less than ±0.08 Hz between ±100 kHz and the AOA with an error of less than ±1.3 deg from 0° to 90° are realized.

2. METHOD

The schematic of the proposed measurement system is shown in Fig. 1. An optical carrier with its polarization state adjusted by a polarization controller (PC, PC1) is sent to a PDM-DMZM. To simulate the scenario of observing a moving object, a transmitted signal (Tx) with an angular of ω_1 is divided into two paths separately fed into the RF ports of the sub-DMZMs. A pair of echo signals ($RX1$ and $RX2$) with an angular frequency of ω_2 and a phase difference of θ are applied into other RF ports of the two DMZMs. Therefore, the modulated signals at the outputs of DMZM1 and DMZM2 can be written as

$$E_x = \sqrt{\frac{P_{\text{in}}}{2}}\sqrt{t_{ff}}[\exp j(\omega_C t + \beta_1 \cos\omega_1 t) + \exp j(\omega_C t + \beta_2 \cos\omega_2 t)], \tag{1}$$

$$E_y = \sqrt{\frac{P_{\text{in}}}{2}}\sqrt{t_{ff}}\{\exp(j\omega_C t + \beta_1 \cos\omega_1 t) + \exp[j\omega_C t + \beta_2 \cos(\omega_2 t + \theta) + j\phi]\}, \tag{2}$$

where ω_C is the angular frequency of the optical carrier, P_{in} represents the optical power, t_{ff} is the insertion loss of two DMZMs, β_1 and β_2 represent the modulation indices of the transmitted and echo signals, and ϕ represents the optical phase difference introduced by a DC voltage applied to DMZM2. θ is the phase difference related to the AOA of the received RF signals, which is given by

$$\theta = \omega_2 \Delta\tau + 2k\pi,$$
$$\varphi = \cos^{-1}(c\Delta\tau/d), \tag{3}$$

where $\Delta\tau$ is the relative time delay between the two received signals, d is the distance of two antennas, c is the light speed, and φ refers to the AOA of the received signals.

According to the Bessel function of the first kind, Eqs. (1) and (2) can be expanded to

$$E_x = \sqrt{\frac{P_{\text{in}}}{2}}\sqrt{t_{ff}}\{jJ_1(\beta_1)\exp[j(\omega_C - \omega_1)t] + J_0(\beta_1)\exp(j\omega_C t) + jJ_1(\beta_1)\exp[j(\omega_C + \omega_1)t] + jJ_1(\beta_2)\exp[j(\omega_C - \omega_2)t] + J_0(\beta_2)\exp(j\omega_C t) + jJ_1(\beta_2)\exp[j(\omega_C + \omega_2)t]\}, \tag{4}$$

$$E_y = \sqrt{\frac{P_{\text{in}}}{2}}\sqrt{t_{ff}}\{jJ_1(\beta_1)\exp[j(\omega_C - \omega_1)t] + J_0(\beta_1)\exp(j\omega_C t) + jJ_1(\beta_1)\exp[j(\omega_C + \omega_1)t] + jJ_1(\beta_2)\exp[j(\omega_C - \omega_2)t - j\theta + j\phi] + J_0(\beta_2)\exp(j\omega_C t + j\phi) + jJ_1(\beta_2)\exp[j(\omega_C + \omega_2)t + j\theta + j\phi]\}. \tag{5}$$

The polarization-multiplexed signal of the PDM-DMZM is sent to an OBPF to filter out the +1st-order sidebands, which is given by

$$\begin{bmatrix} E_x \\ E_y \end{bmatrix} = \sqrt{\frac{P_{\text{in}}}{2}}\sqrt{t_{ff}}\begin{Bmatrix} jJ_1(\beta_1)\exp[j(\omega_C + \omega_1)t] \\ +jJ_1(\beta_2)\exp[j(\omega_C + \omega_2)t] \\ jJ_1(\beta_1)\exp[j(\omega_C + \omega_1)t] \\ +jJ_1(\beta_2)\exp[j(\omega_C + \omega_2)t + j\theta + j\phi] \end{Bmatrix}. \tag{6}$$

By adjusting another PC (PC2) to make the polarization state of the optical signal align to the main axis of a polarization beam splitter (PBS), the polarization-multiplexed optical signal is re-divided into two orthogonal branches. Through the photodetection of the two PDs (PD1 and PD2) connected to the two branches, a dual-channel microwave photonic mixer is achieved, and the two downconverted IF signals can be written as

$$\begin{bmatrix} i_x \\ i_y \end{bmatrix} \propto \begin{bmatrix} \cos(\omega_1 - \omega_2)t \\ \cos[(\omega_1 - \omega_2)t - \theta - \phi] \end{bmatrix} = \begin{bmatrix} \cos\omega_d t \\ \cos(\omega_d t - \theta - \phi) \end{bmatrix} \quad \omega_1 > \omega_2, \quad \text{DFS} > 0$$

or

$$\begin{bmatrix} i_x \\ i_y \end{bmatrix} \propto \begin{bmatrix} \cos(\omega_2 - \omega_1)t \\ \cos[(\omega_2 - \omega_1)t + \theta + \phi] \end{bmatrix} = \begin{bmatrix} \cos\omega_d t \\ \cos(\omega_d t + \theta + \phi) \end{bmatrix} \quad \omega_1 < \omega_2, \quad \text{DFS} < 0 \tag{7}$$

$\omega_d = |\omega_1 - \omega_2|$ represents the value of microwave DFS, which can be obtained by measuring the frequency of the IF signal. Besides, the direction of DFS can be determined by comparing the phase difference $|\theta + \varphi|$ between i_x and i_y. If i_x is ahead of i_y, a positive phase difference and a positive

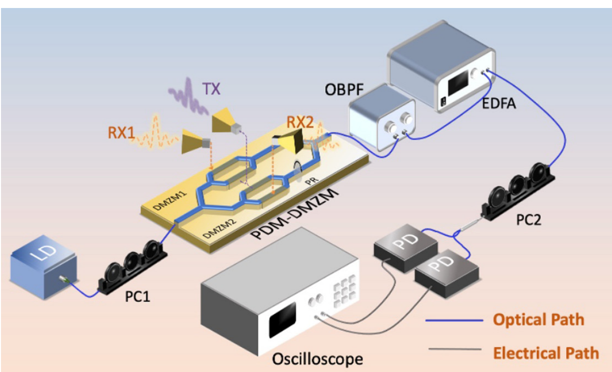

Fig. 1. Schematic of the proposed system. LD, laser diode; PC, polarization controller; DMZM, dual-drive Mach–Zehnder modulator; PDM-DMZM, polarization-division multiplexed DMZM; PR, polarization rotator; OBPF, optical bandpass filter; EDFA, erbium-doped fiber amplifier; PBS, polarization beam splitter; PD, photodetector.

direction of DFS will be obtained. In contrast, a negative phase difference and negative direction will be derived as i_y is ahead of i_x. Furthermore, the value of θ can be obtained when the bias-introduced phase shift ϕ is known after precalibration. It should be noted that, when ϕ is set to be 90°, the proposed dual-channel microwave photonic mixer will be regarded as an I/Q mixer, which is widely used in the previous demonstrations [18]. Unlike in [23], the introduction of ϕ ensures the universality of the proposed system. Even the data come from the perpendicular bisector of the two receiving antennas (i.e., $\theta = 0$ deg), the direction of the DFS can still be distinguished.

3. RESULTS AND DISCUSSION

In a proof-of-concept experiment, a continuous-wave (CW) source with a wavelength of 1550.1 nm and a power of 17.84 dBm is sent to a PDM-DMZM (Fujitsu FTM7980). The modulator has a bandwidth of larger than 20 GHz and a half-wave voltage of less than 3.5 V. The transmitted and echo signals are generated by two microwave sources (Agilent E8257D and Agilent N5183A). After modulation, the output signal of the PDM-DMZM goes through an OBPF (Yenista XTM-50) with the +1st-order sideband selected. The selected sideband is then separated into two orthogonal polarizations by a PC and a PBS. After using two low-frequency PDs with a bandwidth of 150 MHz and a transimpedance gain of 10^3 V/A, the downconverted IF signals are processed by a real-time oscilloscope to measure the DFS and AOA. The optical spectra and electrical spectra are captured by an optical spectrum analyzer (YOKOGAWA AQ6370) and an electrical spectrum analyzer (R&S FSV-40), respectively.

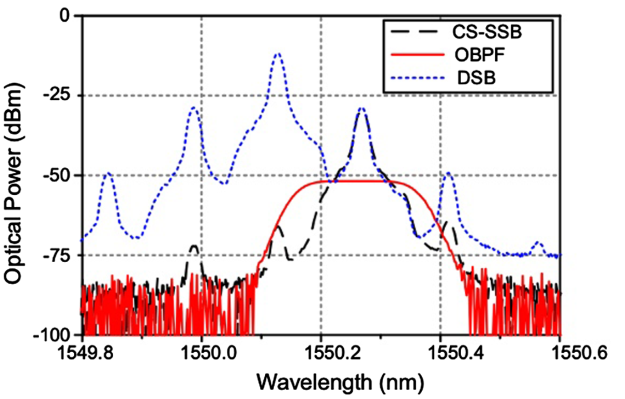

Fig. 2. Optical spectra of the polarization-multiplexed signal before (blue dotted line) and after (black dashed line) the OBPF. Red solid line: frequency response of the OBPF. CS-SSB, carrier suppressed single sideband.

In the experiment, the frequency of the transmitted signal is 10 GHz and that of the echo signal is 10.01 GHz. The power of both the signal is set to be 10 dBm. Figure 2 shows the optical spectra of the modulated signal before and after optical filtering. As can be seen from the red solid line, by properly setting the central wavelength and bandwidth, the optical carrier together with other unwanted optical sidebands are largely suppressed by the OBPF. Only the +1st-order sideband is selected and its power is 30 dB higher than the residual optical carrier and −2nd-order sideband, as depicted as the black dashed line in Fig. 2.

The proposed dual-channel microwave photonic mixer is based on the polarization multiplexing by the PDM-DMZM and the polarization demultiplexing by PC2 and the PBS [27]. To verify this, waveforms at the outputs of PD1 and PD2 when DMZM2 or DMZM1 is separately undriven are measured and shown in Fig. 3. By comparing the waveforms in Fig. 3, we can see that, when adjusting PC2 to make the polarization state of the light align to the main axis of the PBS, the waveform can only be obtained at a single PD, indicating that the polarization-multiplexed optical signal can be effectively separated into two orthogonally polarized branches with neglectable polarization crosstalk. It should be noted that the bias drift of the modulator and the polarization state of PC2 can influence the stability of the system. To maintain good stability, some means can be considered, such as modulator bias-controller [28] and an electrically PC with feedback controlling [29,30].

Figure 4(a) shows the electrical waveforms of the two downconverted IF signals. According to the corresponding spectra shown in Fig. 4(b), the frequency of the downconverted IF signal is 10 MHz, so the DFS value is 10 MHz. Besides, as shown in the waveforms, since the waveform obtained by PD1 is ahead of that by PD2, the DFS direction is positive, according to the description in Eq. (7). When the frequency of the echo signal is changed to be 9.99 GHz, the measured DFS value keeps being 10 MHz, as shown in Fig. 4(d). However, the phase relationship between the two outputs is reversed, as depicted in Fig. 4(c), so a negative DFS direction is derived. To further demonstrate the DFS measurement within a wide frequency range, the frequency of the echo signal is changed within ± 0.001 GHz with a 20 kHz step at 10, 20, 30, and 40 GHz respectively. As

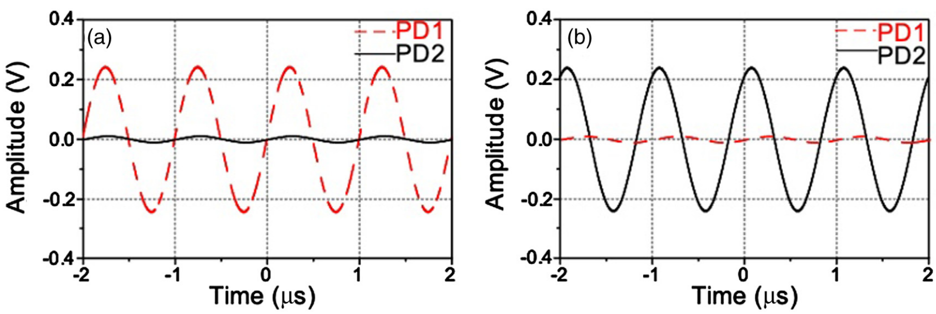

Fig. 3. Obtained electrical waveforms at the outputs of PD1 (red dashed line) and PD2 (black solid line) when (a) DMZM2 or (b) DMZM1 is separately undriven.

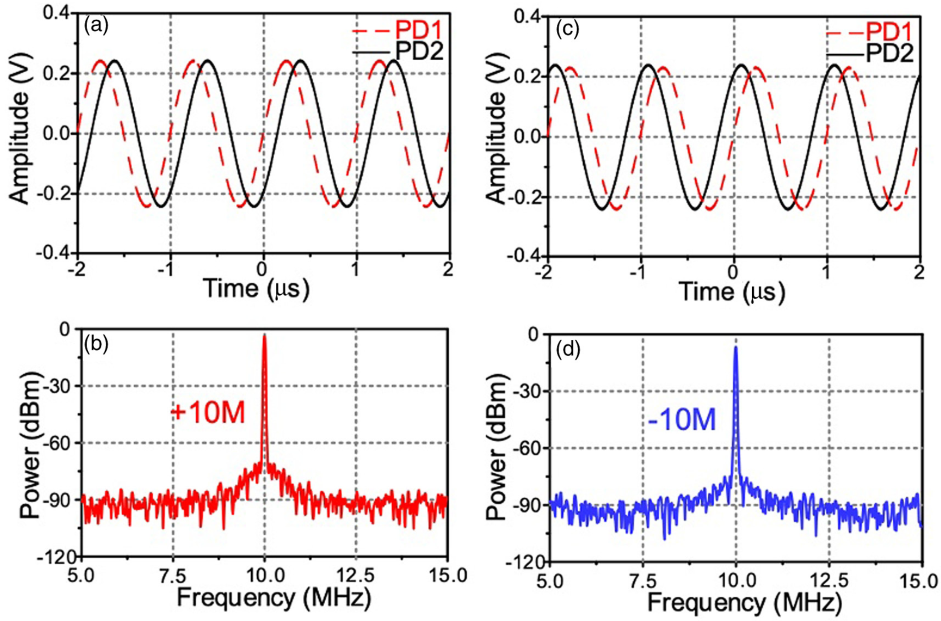

Fig. 4. Electrical (a), (c) waveforms and (b), (d) spectra of downconverted IF signals when the DFS is +10 MHz and −10 MHz, respectively. Red dashed line: downconverted IF signal output from PD1; black solid line: downconverted IF signal output from PD2.

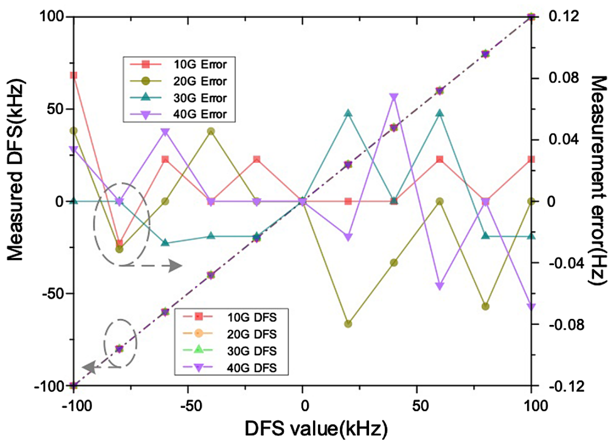

Fig. 5. Measured DFS (black dashed line) and the measurement error (blue solid line) at 10, 20, 30, and 40 GHz.

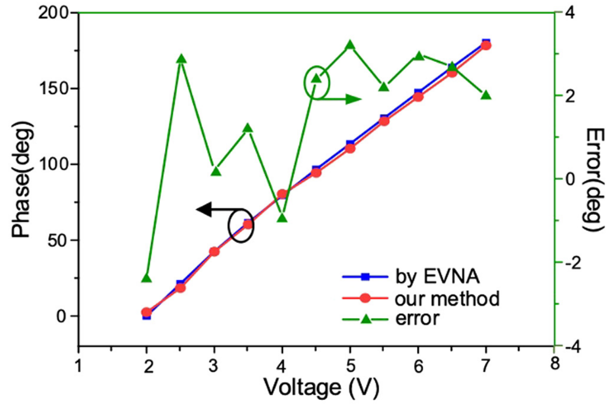

Fig. 6. Phase shifts measured by EVNA (■), the proposed method (•), and the corresponding measurement error of the phase shift (▲).

shown in Fig. 5, when the resolution bandwidth and video bandwidth of the electrical spectrum analyzer are both 1 Hz, all the measurement errors are estimated to be less than $\pm$ 0.08 Hz. Besides, the sensitivity of the system is also discussed. In our experiment, when the power of the transmitted signal is set to be $-5 \sim 10$ dBm, the minimum detectable power of the echo signal is about −90 dBm. When the power of the transmitted signal is gradually reduced to −20, −30, and −40 dBm, the minimum detectable power of the echo signal is increased to −73, −61, and −50 dBm. Similar to the conventional analog photonic link, the sensitivity of the system can be increased by using a lower noise laser, amplifier, and PDs [31].

In order to demonstrate the AOA measurement, a variable phase difference θ is induced by a voltage-controlled microwave phase shifter. The blue-square line (■) in Fig. 6 represents the phase shift with the different applied DC voltages, which is measured by an electrical vector network analyzer (EVNA, R&S ZVA-67), while the red-point line (•) represents the phase shift measured by the proposed AOA measurement system. The measurement error is labeled as the green-triangle line (▲), which is less than $\pm$3.2 deg. According to Eq. (3), we can calculate that the AOA measurement error is less than $\pm$1.3 deg within the angular range from 0° to 90°. It should be stressed here that the stability of MZM states is also necessary for the accurate measurement of AOA according to Eq. (7). The change of the bias state of the MZM will lead to the uncertainty of bias-introduced phase shift ϕ, which will bring ambiguity to the measurement of the AOA. Therefore, the AOA measurement error can be further reduced by introducing a bias controller and temperature controller to the system.

4. CONCLUSION

In conclusion, we propose a microwave-photonics-based DFS and AOA estimation system. Through a dual-channel microwave photonic mixer, the DFS and AOA information can be calculated by the frequency of the downconverted IF signal and the phase difference between them, respectively. Experimental results show that the error of the DFS measurement within ± 100 kHz is less than ± 0.08 Hz, and the error of the AOA measurement ranging from $0°$ to $90°$ is less than ± 1.3 deg. The proposed system provides a reliable solution for future applications such as intelligent driving, wireless communication, radar detection, and other fields.

Funding. National Natural Science Foundation of China (61604072, 62001218); National Key Research and Development Program of China (2020YFB1805704); Natural Science Foundation of Jiangsu Province (BK20200436); Fundamental Research Funds for the Central Universities.

Disclosures. The authors declare no conflicts of interest.

Data Availability. Data underlying the results presented in this paper are not publicly available at this time but may be obtained from the authors upon reasonable request.

REFERENCES

1. S. Patole, M. Torlak, D. Wang, and M. Ali, "Automotive radars: a review of signal processing techniques," IEEE Signal Process. Mag. **34**(2), 22–35 (2017).
2. J. Xiao, X. Li, Y. Xu, Z. Zhang, L. Chen, and J. Yu, "W-band OFDM photonic vector signal generation employing a single Mach-Zehnder modulator and precoding," Opt. Express **23**, 24029–24034 (2015).
3. F. Laghezza, F. Scotti, P. Ghelfi, and A. Bogoni, "Photonics-assisted multiband RF transceiver for wireless communications," J. Lightwave Technol. **32**, 2896–2904 (2014).
4. J. Hasch, E. Topak, R. Schnabel, T. Zwick, R. Weigel, and C. Waldschmidt, "Millimeter-wave technology for automotive radar sensors in the 77 GHz frequency band," IEEE Trans. Microw. Theory Tech. **60**, 845–860 (2012).
5. D. M. Grimes and T. O. Jones, "Automotive radar: a brief review," Proc. IEEE **62**, 804–822 (1974).
6. P. Ghelfi, F. Laghezza, F. Scotti, G. Serafino, A. Capria, S. Pinna, and A. Bogoni, "A fully photonics-based coherent radar system," Nature **507**, 341–345 (2014).
7. F. Zhang, Q. Guo, and S. Pan, "Photonics-based real-time ultra-high-range-resolution radar with broadband signal generation and processing," Sci. Rep. **7**, 13848 (2017).
8. N. Sharma and L. M. Aggarwal, "Automated medical image segmentation techniques," J. Med. Phys. **35**, 3–14 (2010).
9. J. Yao, "Microwave photonics," J. Lightwave Technol. **27**, 314–335 (2009).
10. X. Zou, W. Li, B. Lu, W. Pan, L. Yan, and L. Shao, "Photonic approach to wide-frequency-range high-resolution microwave/millimeter-wave Doppler frequency shift estimation," IEEE Trans. Microw. Theory Tech. **63**, 1421–1430 (2015).
11. S. Pan and J. Yao, "Photonics-based broadband microwave measurement," J. Lightwave Technol. **35**, 3498–3513 (2017).
12. S. Pan and Y. Zhang, "Microwave photonic radars," J. Lightwave Technol. **38**, 5450–5484 (2020).
13. S. Pan, X. W. Ye, Y. M. Zhang, and F. Z. Zhang, "Microwave photonic array radar," IEEE J. Microw. **1**, 176–190 (2021).
14. J. Li, J. Xiao, X. Song, Y. Zheng, C. Yin, Q. Lv, Y. Fan, F. Yin, Y. Dai, and K. Xu, "Full-band direct-conversion receiver with enhanced port isolation and I/Q phase balance using microwave photonic I/Q mixer (invited paper)," Chin. Opt. Lett. **15**, 010014 (2017).
15. P. Wu, X. Han, Y. Gu, S. Li, S. Hu, and M. Zhao, "Novel photonic approach to microwave frequency measurement using tunable group delay line," Chin. Opt. Lett. **9**, 081301 (2011).
16. B. Lu, W. Pan, X. Zou, X. Yan, L. Yan, and B. Luo, "Wideband Doppler frequency shift measurement and direction ambiguity resolution using optical frequency shift and optical heterodyning," Opt. Lett. **40**, 2321–2324 (2015).
17. L. Xu, Y. Yu, H. Tang, and X. Zhang, "A simplified photonic approach to measuring the microwave Doppler frequency shift," IEEE Photon. Technol. Lett. **30**, 246–249 (2017).
18. C. Huang, E. H. Chan, and C. B. Albert, "Wideband DFS measurement using a low-frequency reference signal," IEEE Photon. Technol. Lett. **31**, 1643–1646 (2019).
19. W. Chen, A. Wen, X. Li, Y. Gao, Y. Wang, S. Xiang, and H. Zheng, "Wideband Doppler frequency shift measurement and direction discrimination based on a DPMZM," IEEE Photon. J. **9**, 5501008 (2017).
20. B. Vidal, M. A. Piqueras, and J. Marti, "Direction-of-arrival estimation of broadband microwave signals in phased-array antennas using photonic techniques," J. Lightwave Technol. **24**, 2741–2745 (2006).
21. Z. Cao, Q. Wang, R. R. Lu, V. D. Boom, E. Tangdiongga, and A. T. Koonen, "Phase modulation parallel optical delay detector for microwave angle-of-arrival measurement with accuracy monitored," Opt. Lett. **39**, 1497–1500 (2014).
22. H. Chen and E. H. W. Chan, "Simple approach to measure angle of arrival of a microwave signal," IEEE Photon. Technol. Lett. **31**, 1795–1798 (2019).
23. H. Chen and E. H. Chan, "Photonics-based CW/pulsed microwave signal AOA measurement system," J. Lightwave Technol. **38**, 2292–2298 (2020).
24. P. Li, L. Yan, J. Ye, X. Feng, W. Pan, B. Luo, and Z. Chen, "Photonic approach for simultaneous measurements of Doppler-frequency-shift and angle-of-arrival of microwave signals," Opt. Express **27**, 8709–8716 (2019).
25. Z. Tang and S. Pan, "Simultaneous measurement of Doppler-frequency-shift and angle-of-arrival of microwave signals for automotive radars," in *International Topical Meeting on Microwave Photonics (MWP)* (2019), pp. 1–4.
26. C. Huang, H. Chen, and E. H. Chan, "Simple photonics-based system for Doppler frequency shift and angle of arrival measurement," Opt. Express **28**, 14028–14037 (2020).
27. Z. Tang and S. Pan, "Image-reject mixer with large suppression of mixing spurs based on a photonic microwave phase shifter," J. Lightwave Technol. **34**, 4729–4735 (2016).
28. Y. Fu, X. Zhang, B. Hraimel, T. Liu, and D. Shen, "Mach–Zehnder: a review of bias control techniques for Mach–Zehnder modulators in photonic analog links," IEEE Microwave Mag. **14**(7), 102–107 (2013).
29. Z. Chen, L. Yan, H. Jiang, W. Pan, B. Luo, and X. Zou, "Dispersion compensation in analog photonic link utilizing a phase modulator," J. Lightwave Technol. **32**, 4642–4647 (2014).
30. M. Martinelli, P. Martelli, and S. M. Pietralunga, "Polarization stabilization in optical communications systems," J. Lightwave Technol. **24**, 4172–4183 (2006).
31. X. Xie, K. Li, Q. Zhou, A. Beling, and J. C. Campbell, "High-gain low-noise-figure and high-linearity analog photonic link based on a high-performance photodetector," J. Lightwave Technol. **32**, 4187–4192 (2014).